Available online at www.sciencedirect.com
SCIENCE DIRECT®
Journal of Molecular Spectroscopy 226 (2004) 146–160
Journal of MOLECULAR SPECTROSCOPY
www.elsevier.com/locate/jms

High sensitivity cw-cavity ringdown and Fourier transform absorption spectroscopies of $^{13}CO_2$ ☆

Y. Ding,[a,b] P. Macko,[a,c] D. Romanini,[a] V.I. Perevalov,[d] S.A. Tashkun,[d] J.-L. Teffo,[e] S.-M. Hu,[b] and A. Campargue[a,*]

[a] *Laboratoire de Spectrométrie Physique (associated with CNRS, UMR 5588), Université Joseph Fourier de Grenoble, B.P. 87, 38402 Saint-Martin-d'Hères Cedex, France*
[b] *Laboratory of Bond-Selective Chemistry, University of Science and Technology of China, Hefei 230026, PR China*
[c] *Faculty of Mathematics, Physics and Informatics, Comenius University, Mlynská dolina, 84248 Bratislava, Slovakia*
[d] *Laboratory of Theoretical Spectroscopy, Institute of Atmospheric Optics, SB, Russian Academy of Science, 1, Akademicheckii av., 634055 Tomsk, Russia*
[e] *Laboratoire de Physique Moléculaire et Applications, C.N.R.S., Case 76, Université Pierre et Marie Curie, 4 Place Jussieu, 75252 Paris Cedex 05, France*

Received 21 January 2004; in revised form 5 March 2004
Available online 24 April 2004

Abstract

The absorption spectrum of $^{13}CO_2$ has been recorded by cw-cavity ringdown spectroscopy with a new set up based on fibered DFB lasers. By using a series of 31 DFB lasers, the spectrum of carbon dioxide could be recorded in the 6130–6750 cm^{-1} region with a typical sensitivity of 5×10^{-10} cm^{-1}. The spectrum has also been recorded between 4400 and 8500 cm^{-1} with a Fourier transform spectrometer associated with a multi-pass cell (maximum path length of 105 m). The new observations obtained both by FTS and CRDS represent a significant extension of the available data. For instance, more than 4000 line positions were measured and assigned in the CRDS spectrum while only 232 line positions are listed in the HITRAN database. Altogether, the band by band analysis has led to the determination of the rovibrational parameters of 65, 7, and 24 bands for the $^{13}C^{16}O_2$, $^{16}O^{13}C^{17}O$, and $^{16}O^{13}C^{18}O$ isotopomers, respectively. As some observed line positions show significant deviations from the predictions of the effective Hamiltonian model, the new observed line positions were gathered with the data available in the literature to refine the set of effective Hamiltonian parameters of the $^{13}C^{16}O_2$ isotopic species. The refined set of 96 effective Hamiltonian parameters reproduces more than 14 650 line positions of $^{13}C^{16}O_2$ with an RMS = 0.002 cm^{-1}. A detailed comparison with the line positions retrieved from Venus spectra and the line list provided by HITRAN is also presented and discussed.

Keywords: $^{13}CO_2$; Cavity ringdown spectroscopy; Fourier transform spectroscopy; Effective Hamiltonian model

1. Introduction

Carbon dioxide is a minor atmospheric compound of first importance. As a result of human activity (in particular combustion), its concentration has continuously increased during the last century. Carbon dioxide is the second green house gas after atmospheric water; it contributes then greatly to the global warming of the atmosphere. This issue, of fundamental importance for the present and the future of mankind, constitutes the first climate change of anthropogenic origin.

The present work aims to a better knowledge and understanding of the absorption of $^{13}CO_2$ which is the second most abundant isotopomer after $^{12}CO_2$ (natural abundance 1.1%). Fourier transform spectroscopy (FTS) associated with a multi-pass gas cell has been used for recording the absorption spectrum over the wide spectral range 4400–8500 cm^{-1}. The good

☆ Supplementary data for this article are available on ScienceDirect (www.sciencedirect.com) and as part of the Ohio State University Molecular Spectroscopy Archives (http://msa.lib.ohio-state.edu/jmsa_hp.htm).

* Corresponding author. Fax: +33-4-76-63-54-95.
E-mail address: alain.campargue@ujf-grenoble.fr (A. Campargue).

0022-2852/$ - see front matter © 2004 Elsevier Inc. All rights reserved.
doi:10.1016/j.jms.2004.03.009

sensitivity achieved in these recordings ($\alpha_{min} = 10^{-7}\,cm^{-1}$) has allowed to detect 36 bands of $^{13}C^{16}O_2$, nine of them being newly reported and the analysis of the other being improved. Indeed, as indicated by the HITRAN database [1], there is a lack of laboratory measurements (in particular intensities) of weak near infrared absorption bands of carbon dioxide. In the considered spectral region, most of the spectroscopic constants were obtained from the analysis by Mandin [2] of the high resolution spectrum of Venus atmosphere, recorded in 1973 by Connes and Michel [3]. In these conditions of pressure and optical path, very weak transitions could be detected but the analysis of the spectra were complicated by line overlapping and the correction of the Doppler effects resulting both of the relative translation of the Earth and of Venus and of the rotation of the Earth.

Laboratory investigations of weak overtone or combination bands of carbon dioxide at high spectral resolution require high sensitive techniques. In particular, we have applied to the $^{12}CO_2$ species, the intracavity laser absorption spectroscopy (ICLAS) technique above $9000\,cm^{-1}$ (see [4] and the review of the observed transitions above $10\,000\,cm^{-1}$ given in [5]). For instance, compared to laboratory measurements around 1 μm [4], a shift of the order of $10^{-2}\,cm^{-1}$ was evidenced in the wavenumber calibration of $^{12}CO_2$ bands observed in the Venus spectra, allowing for a significant improvement of the consistency of the analysis of the atmospheric spectrum in this spectral region [6]. In the present work, to fully characterize the spectrum near 1.5 μm corresponding to an atmospheric transparency window, the spectrum has been recorded by using cw-cavity ringdown spectroscopy (CRDS). The use of a set of 31 DFB laser diodes for cw-CRDS has allowed a full coverage of the 6130–6750 cm^{-1} spectral region, not easily accessible by ICLAS, with a sensitivity better than $10^{-9}\,cm^{-1}$. The performances of this set up result in a considerable improvement of the knowledge of the spectrum in this region: while only 7 bands of $^{13}C^{16}O_2$ were identified from the Venus spectrum, we could rotationally assign 2653 transitions to 39 bands. The improvements concern also the minor asymmetric isotopomers $^{16}O^{13}C^{18}O$ and $^{16}O^{13}C^{17}O$ present in our sample for which a total of 13 and 3 bands were detected, respectively, compared to 1 and 0 in the Venus spectrum.

The assignment of the spectrum has been performed with the help of the predictions of the effective Hamiltonian developed in our papers [7,33] which show a very good agreement with the observations. But in the case of the $^{13}C^{16}O_2$ isotopic species, a few bands show significant deviations. We then decided to perform a new global fitting of the line positions of this isotopic species by gathering the present line positions with previous measurements [7–28] and line positions recently obtained by ICLAS above $10\,000\,cm^{-1}$ [5].

2. Experiment

2.1. Fourier transform spectroscopy

The absorption spectrum of carbon dioxide enriched with ^{13}C has been recorded at room temperature between 4400 and $8500\,cm^{-1}$ with a Bruker IFS 120HR Fourier transform spectrometer equipped with a path length adjustable multi-pass gas cell. The maximum optical path length is 105 m. The sample was purchased from Aldrich Chemical. The section of the FT spectrum corresponding to the CRDS region is presented in Fig. 1. The stated isotopic concentration is 99% of ^{13}C for carbon atom and less than 3% of ^{18}O for oxygen atom. A mass spectroscopy experiment has given the following isotopic abundance in the sample: $^{13}C^{16}O_2$ 95.3%, $^{16}O^{13}C^{18}O$ 2.4%, $^{12}C^{16}O_2$ 1.8%, and $^{16}O^{13}C^{17}O$ 0.5% which leads to an ^{18}O enrichment value of 1.2% which was roughly confirmed on the basis of intensity measurements. Because of the wide spectral range and the large variation of the absorption line intensities, spectra were recorded under different experimental conditions listed in Table 1. A tungsten source, CaF_2 beam splitter were used in all experiments. The line positions were calibrated using those of $^{12}C^{16}O_2$ listed in HITRAN database [1]. The accuracy of line positions of unblended and not-very-weak lines is estimated to be better than $0.001\,cm^{-1}$.

2.2. Cavity ringdown spectroscopy

The principles of the implementation of cw lasers for CRDS were first demonstrated with a dye laser or an external cavity diode laser. The cw-CRDS technique has already been described in much detail [29,30]. With

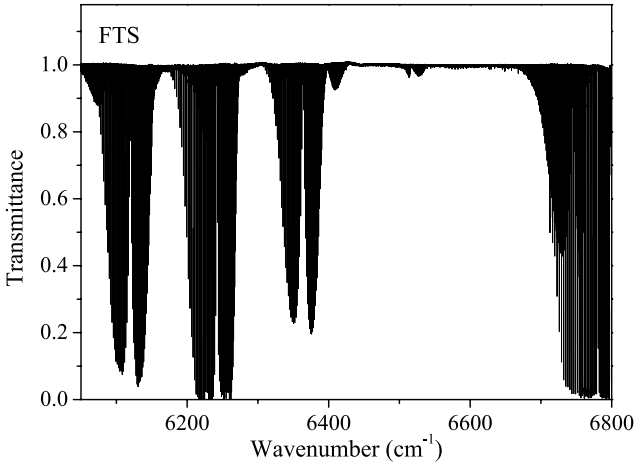

Fig. 1. Overview of the FTS spectrum of ^{13}C enriched carbon dioxide in the 6100–6800 cm^{-1} region explored by cw-CRDS. Experimental conditions: spectral resolution $0.01\,cm^{-1}$, Ge detector, total gas pressure 3213 Pa and absorption path length 105 m.

Table 1
Experimental conditions used to record the Fourier transform absorption spectra of ^{13}C enriched carbon dioxide

Spectral region (cm^{-1})	Pressure (Pa)	Detector	Path length (m)	Resolution (cm^{-1})	Scan No.
4400–5050	50.2	InSb[a]	15	0.005	469
4400–5050	1089	InSb[a]	15	0.005	690
4400–7600	2433	InSb[a]	69	0.01	1340
5500–9500	3213	Ge	105	0.01	2546
6000–8000	389	InSb[a]	15	0.007	658

[a] Liquid-nitrogen cooled.

respect to the fibered DFB laser setup used here (Fig. 2), it was presented in detail more recently [37], and therefore we describe here only the main features. For this setup, we used fibered components wherever possible, which can be easily connected together (we used components with low-feedback FC/APC connectors). To cover the near infrared atmospheric window near 1.5 μm without any gap, 31 fibered DFB lasers from three industry-leading manufacturers (NEL, Lucent, and Alcatel) were used. These butterfly-packaged telecom DFB lasers, which include a 30 dB optical isolator, are today available for few hundred Euros at any specified wavelength in the range 1480–1630 nm. They produce about 20 mW for several years of continuous operation, and the packaging includes a Peltier and a thermistance for laser temperature stabilization and a power monitoring photodiode. The DFB typical tuning range is about 1 nm by current tuning and 7 nm (about 30 cm^{-1}) by temperature tuning from −5 °C to 60 °C (0.1 nm/°C).

In our setup, an additional fibered optical isolator is connected to the laser, followed by a fibered acousto-optic switch (AOS). All open-path optics are placed on a linear rail 2 m long, with a single-mode fiber delivering laser radiation to one end of the vacuum-tight ringdown cell, which is 140 cm long. A single lens images the diverging fiber output into the TEM_{00} cavity mode. The cavity output is focused on a sensitive InGaAs avalanche photo-diode (APD) (model Epitaxx ETX240). The cavity mirrors ($R = 1$ m) are mounted on tilt stages, one of which includes a piezoelectric tube for modulating the cavity length by slightly more than $\lambda/2$. This makes the cavity modes oscillate by more than one FSR thus producing a passage through resonance with the laser line twice per modulation cycle. The maximum modulation rate permitted by our high-voltage oscillator is about 500 Hz, which gives a maximum ringdown repetition rate of 1 kHz. The effective data rate is somewhat lower since a fraction of passages through resonance may fail to go above the threshold which triggers the AOS shut-down period (a typical APD signal observed is displayed in Fig. 2).

A program running under DOS insures laser diode tuning by temperature steps, and real-time calculation of the ringdown rate from the digitized APD signal at a repetition rate compatible with the cavity modulation (up to 1 kHz). About 100 ringdown events were averaged for each spectral data point, and about 30 min were needed to complete a temperature scan for each DFB laser. Changing from a laser to the next required a few minutes, so that the whole spectral range covered by a mirror set (about half of the total range) could be completed in 1 day (∼15 scans). More time was then needed for changing mirror set, realign the cavity and refill the cell. We plan to purchase super-mirrors centered at 1550 nm which will thus cover the whole range at once.

We used two pairs of the super mirrors, one pair working between 1480 and 1560 nm and other between 1550 and 1630 nm. The ringdown time varied from 30 to 90 μs depending on the laser wavelength. The cor-

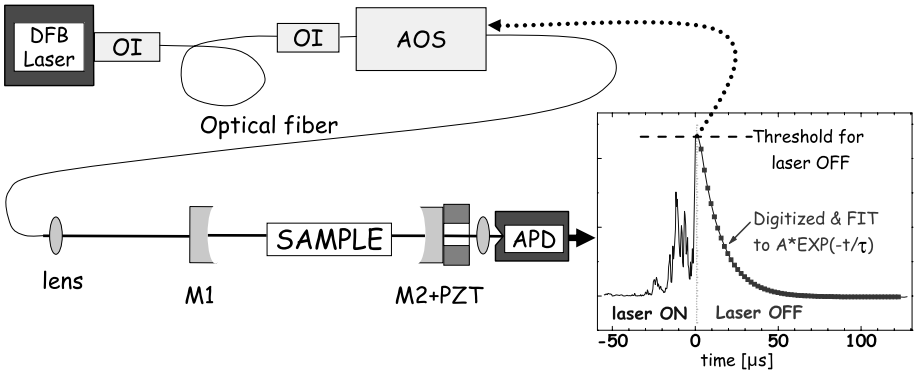

Fig. 2. Fibered cw-CRDS setup: OI is an optical isolator, AOS an acousto-optic switch, APD an avalanche photo-diode, PZT a piezoelectric transducer, M1 and M2 are the cavity supermirrors. On the right, is displayed a typical cavity output signal, recorded during a passage through resonance: a noisy cavity build-up is observed, which then gives a clean exponential ring-down when the laser is shut off by the AOS (see [37]).

responding noise level on the spectrum baseline varied from 1×10^{-9} to $3 \times 10^{-10}\,cm^{-1}$, respectively. The sensitivity of the FTS and cw-CRDS experiments is illustrated in Fig. 3 in the region of the band head of the *R* branch of the 11121–00001 band. The typical noise level in the FTS spectrum is $(\alpha l)_{min} \sim 10^{-3}$ which, for a path length of $l = 105\,m$, leads to a sensitivity of $10^{-7}\,cm^{-1}$.

The vacuum ringdown cell was made from a stainless steel tube of 10 mm inner diameter. Before the measurement, the tube was pumped by a rotary oil pump to a pressure of few mTorr and filled afterwards. We used a CO_2 sample identical to the one used for the FTS recordings. The gas pressure, measured by a capacitance gauge (Baratron), as well as the ringdown cell temperature, were monitored during the spectrum recording. A typical pressure value of 26 hPa (20 Torr) was adopted.

As mentioned above, each DFB laser allows the recording of a 30–40 cm^{-1} wide spectral region whose wavenumber calibration was performed independently. The procedure consisted, first, of correcting the nonlinearity of the frequency tuning of the laser. For this purpose, a fraction of the laser beam was deflected on an étalon by a 1% fibred coupler, and the transmitted signal was recorded simultaneously with the spectrum. This étalon signal helped to identify eventual laser mode-hops, however, only one out of our 31 DFBs showed some instabilities when tuning at temperatures higher than 46 °C. After linearization of the wavenumber scale, the spectrum was absolutely calibrated using accurate values of water (present in our sample as impurity) or $^{12}CO_2$ line positions given in the HITRAN database [1]. The Fourier transform spectra were also used to calibrate the CRDS spectra in the region where no accurate water or $^{12}CO_2$ line positions were available. We estimate our wavenumber calibration to be better than $0.002\,cm^{-1}$ as confirmed by (i) the comparison of the line positions measured in the overlapping spectral region corresponding to two successive DFB lasers and (ii) the rotational analysis (see below) which leads to RMS values generally better than $0.002\,cm^{-1}$ while line positions of a given band generally spreads over several spectral sections which were calibrated independently.

3. Rotational analysis and vibrational assignment

The standard expression were used for the vibration–rotational energy levels of the upper and lower states

$$T_v = G_v(v_1, v_2^{\ell_2}, v_3) + F_v(J), \tag{1}$$

where G_v and F_v are the vibrational and rotational contributions, respectively, with

$$F_v(J) = B_v[J(J+1) - k^2] - D_v[J(J+1) - k^2]^2 + H_v[J(J+1) - k^2]^3, \tag{2}$$

where $k = \ell_2$ is the quantum number associated to the vibrational angular momentum.

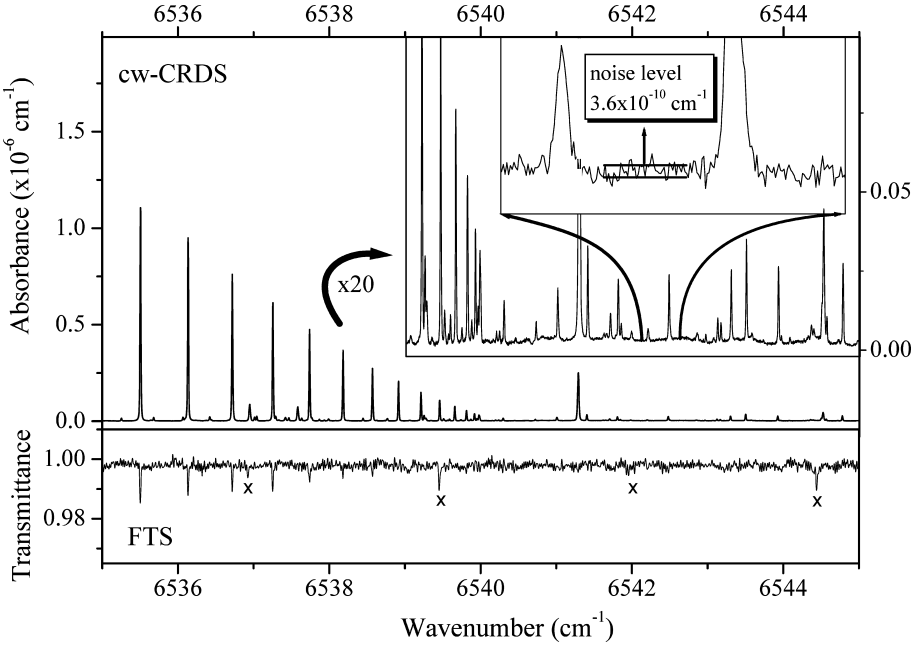

Fig. 3. Comparison of the CRDS and FTS spectra between 6535 and 6545 cm^{-1} showing the band head of the *R* branch of the 11121–00001 band centered at 6515.120 cm^{-1}. Two successive enlargements show the typical sensitivity achieved by cw-CRDS: the noise level corresponding to the minimum value of the absorption coefficient which can be detected is about $4 \times 10^{-10}\,cm^{-1}$. The four lines marked by 'x' correspond to strong acetylene transitions present as a trace in the FTS cell. The pressure was 26 hPa.

In the fitting procedure, the rotational constants of the ground state -B'', D'', and H''-, were constrained to their literature values [31] and the quantities ΔG_v, ΔB_v, ΔD_v, and ΔH_v (in a few cases) were fitted. A complete list of the assigned rotational lines is attached to the paper as supplementary data. The spectrum analysis was greatly helped by the line positions accurately predicted by the effective Hamiltonians developed for the three isotopomers contributing to our spectrum: $^{13}C^{16}O_2$ [7], $^{16}O^{13}C^{17}O$ [32], and $^{16}O^{13}C^{18}O$ [33]. These effective Hamiltonians are based on that used by Chédin [32]. The predicted line intensities were also considered in the spectrum analysis. For these calculations, the effective dipole moment parameters of the main isotopic species [34] were used. In the case of the weakest bands, combination difference relations were systematically used to identify the isotopomer and the lower vibrational state of the observed transitions. We present hereafter, for each isotopomer, the new spectroscopic information retrieved from the FTS and CRDS spectra.

3.1. $^{13}C^{16}O_2$

Sixteen cold bands and twenty hot bands could be assigned to the $^{13}C^{16}O_2$ species in the FTS spectrum (4400–8500 cm^{-1} region) while seven cold bands, thirty hot bands, and two $\Delta l_2 = 2$ forbidden bands, could be assigned to the $^{13}C^{16}O_2$ species in the CRDS spectrum between 6130 and 6750 cm^{-1}. The spectroscopic parameters retrieved from the fitting of the line positions are presented in Tables 2 and 3 for the FTS and CRDS spectra, respectively. We use in these Tables the HITRAN notation [1] for the labelling of the vibrational levels. The bands listed in bold character in Table 3 are those also observed in our FTS spectrum (Table 2), their spectroscopic parameters were generally improved by including in the fit, transitions with higher J values observed in the CRDS spectrum only. As a general rule, for the bands observed both by FTS and cw-CRDS, the "CRDS" parameters (Table 3) were obtained by adding to the "FTS" input data, the line positions of the lines observed in the CRDS spectrum only. This choice was motivated by the fact that, in many cases, the lines observed in the FTS spectrum were saturated in the CRDS spectrum and that the FTS line positions are probably slightly more accurate than the line positions obtained from the CRDS spectra. In the Supplementary Material, a label is given for each line to indicate from which spectrum (FTS or CRDS) the line position was measured. The same remark holds for the bands of the two other isotopomers presented hereafter.

The bands previously observed in the spectrum of Venus atmosphere are marked by "V" in Tables 2–6. Their spectroscopic parameters are improved as a result of the improved accuracy of the line positions and of the detection of transitions with higher J values.

Overall a total number of 2431 lines with J values up to 78 could be rovibrationally assigned to the $^{13}C^{16}O_2$ species in the FTS spectrum. Except for the weakest bands, the observed transitions could be reproduced with an RMS less than 0.001 cm^{-1}, close to the experimental uncertainty.

A section of the FTS and cw-CRDS spectra is compared in Fig. 4. In this region, only the strong 31111–01101 hot band is observed in the FTS spectrum while lines belonging to five weaker bands are detected in the CRDS spectrum. Overall a total number of 2653 lines with J values up to 78 could be rovibrationally assigned in the CRDS spectrum. Except for the few perturbed bands and the weakest bands, the observed transitions could be reproduced with an RMS less than 0.002 cm^{-1}, close to the experimental uncertainty.

In the CRDS region, all but seven bands were found unperturbed. As an example of perturbation, the rotational structure of the 32211 state above $J' > 35$ is illustrated by the reduced energy plot presented in Fig. 5 obtained from the analysis of the 32211–02201 band. On the basis of the effective Hamiltonian [7], the perturbation is identified as resulting from the Coriolis interaction with the 21122 state in full agreement with the observation of some extra lines assigned to the 21122–02201 transitions. The same kind of Coriolis interaction was found to couple the e levels of the 41111 state and that of the 30022 state leading to the observation of extra lines belonging to the 30022–11101 transition. In this particular case, the difference between the observed and predicted [7] line positions reaches values of about 0.03 cm^{-1} which is larger than the experimental uncertainty but shows that the effective Hamiltonian is a powerful tool in the analysis of perturbations. The extra lines are included in the supplementary data. Perturbations are also present for high J values in five other bands marked in Table 3.

3.2. $^{16}O^{13}C^{17}O$

Six bands of $^{16}O^{13}C^{17}O$ were detected in the FTS spectrum between 4500 and 6800 cm^{-1}. Their spectroscopic parameters are presented in Table 4. The 00021–00001 and 20013–00001 bands were previously observed in Venus spectra [2]. A good agreement is obtained for the parameter values of the first band but a strong discrepancy with Mandin's results is observed for the 20013–00001 transition. The line by line comparison shows that the line positions agree and that the discrepancy is due to a shift of one unit in the J value assignment adopted in [2].

From the cw-CRDS spectrum, one extra band could be analysed and the rotational analysis of the bands at 6188.05 and 6752.415 cm^{-1} could be improved. The corresponding spectroscopic parameters retrieved from the fitting of the transitions are gathered in Table 5.

Table 2
Spectroscopic parameters (in cm^{-1}) of $^{13}C^{16}O_2$ bands obtained from the analysis of the FT spectrum between 4400 and 8500 cm^{-1}

$^{13}C^{16}O_2$		υ_0	G_v	B_v	$D_v \times 10^7$	$H_v \times 10^{13}$	J_{max} $P/Q/R$	n/N[a]	RMS $\times 10^4$
22213*e*–02201*e*	V	4673.67745 (29)	5972.50034	0.3899120 (10)	1.0533 (70)		42/ /40	33/37	7.5
22213*f*–02201*f*	V	4673.67756 (29)	5972.50047	0.38990858 (90)	1.6904 (51)		43/ /41	35/38	8.3
31102*e*–00001	V	4683.13389 (66)	4683.52313	0.38923573 (14)	1.3186 (62)		48/ /48	31/36	13.8
30014–10002	V	4685.77329 (20)	5951.60107	0.38963708 (55)	2.2849 (27)		50/ /46	43/45	6.8
21113*e*–01101*e*	V	4708.52559 (16)	5357.39225	0.38862814 (32)	1.6256 (11)	0.376 (11)	55/ /57	54/57	5.9
21113*f*–01101*f*	V	4708.52609 (14)	5357.39423	0.39010321 (26)	1.71368 (84)		56/ /60	53/56	5.5
20013–00001	V	4748.059884 (63)	4748.05988	0.388854328 (90)	1.88624 (23)	9.77 (35)	66/ /70	63/67	2.7
30013–10001		4749.55836 (26)	6119.62047	0.38759094 (79)	1.9700 (45)		44/ /40	35/39	7.4
30013–10002		4853.79266 (12)	6119.62004	0.38758964 (28)	1.7794 (11)		52/ /50	43/44	4.4
21112*e*–01101*e*[b]	V	4871.44131 (44)	5520.30642	0.38707888 (82)	1.3265 (28)		61/ /63	54/61	16.8
21112*f*–01101*f*[b]	V	4871.44296 (25)	5520.30922	0.38822362 (42)	1.3170 (12)	−13.5 (14)	60/ /62	57/58	9.9
30012–10001		4871.90635 (17)	6241.96846	0.38585908 (37)	1.1142 (14)		52/ /54	42/43	6.4
20012–00001	V	4887.38499 (13)	4887.38499	0.38685532 (13)	1.51688 (22)	6.15 (68)	78/ /78	78/78	6.0
30012–10002		4976.14110 (20)	6241.96888	0.38585691 (49)	1.1040 (21)		50/ /50	40/42	6.8
20011–00001[c]	V	4991.35166 (17)	4991.35166	0.38671273 (24)	0.96436 (60)		72/ /76	65/73	7.2
30011–10001[c]		4993.55918 (11)	6363.62129	0.38702693 (33)	0.8662 (17)		50/ /50	40/46	3.6
21111*e*–01101*e*[b]	V	5013.78191 (14)	5662.64680	0.38686278 (21)	1.13342 (54)		61/ /65	58/59	5.7
21111*f*–01101*f*[b]	V	5013.78164 (12)	5662.64753	0.38795468 (18)	1.06605 (48)		64/ /60	57/58	4.5
22211*e*–02201*e*	V	5028.77466 (19)	6327.59037	0.38811627 (31)	1.3554 (13)		42/ /50	37/39	4.3
22211*f*–02201*f*	V	5028.77491 (13)	6327.59062	0.38811436 (29)	1.1465 (11)		43/ /51	34/40	4.0
30011–10002		5097.79333 (24)	6363.62111	0.38702748 (88)	0.8689 (58)		34/ /40	36/38	8.0
01121*e*–00001	V	5168.59937 (10)	5168.98412	0.38474908 (23)	1.34139 (90)		50/ /52	46/50	3.7
01121*f*–00001		5168.59951 (16)	5168.98486	0.38534323 (32)	1.3496 (12)		/54/	27/27	4.3
31114*e*–01101*e*	V	5904.44656 (57)	6553.31366	0.3890685 (21)	1.751 (14)		37/ /37	26/34	12.1
31114*f*–01101*f*	V	5904.44763 (69)	6553.31662	0.3909499 (25)	1.960 (17)		36/ /38	19/35	17.7
30014–00001	V	5951.60162 (16)	5951.60162	0.38963557 (44)	2.2729 (22)		48/ /50	46/50	5.8
31113*e*–01101*e*	V	6088.21449 (18)	6737.07988	0.38736162 (40)	1.5366 (16)		49/ /51	48/49	6.4
31113*f*–01101*f*	V	6088.21456 (13)	6737.08151	0.38890763 (32)	1.6706 (15)		48/ /46	46/46	4.5
30013–00001	V	6119.62083 (23)	6119.62083	0.38758649 (40)	1.7590 (12)		60/ /64	59/63	9.2
30012–00001	V	6241.96832 (15)	6241.96832	0.38586864 (22)	1.10623 (57)		64/ /64	65/65	6.5
31112*e*–01101*e*[d]	V	6243.57210 (16)	6892.43654	0.38640855 (42)	1.2695 (19)		49/ /47	43/48	5.6
31112*f*–01101*f*[d]	V	6243.57233 (24)	6892.43810	0.38773517 (58)	1.2709 (25)		50/ /50	40/44	7.8
41101*e*–00001		6257.01937 (47)	6257.40875	0.38937286 (98)	1.1050 (41)		46/ /48	28/33	9.8
30011–00001[c]	V	6363.62105 (14)	6363.62105	0.38702816 (38)	0.8710 (18)		62/ /60	48/62	5.2
31111*e*–01101*e*	V	6397.54951 (24)	7046.41441	0.38684402 (62)	0.9869 (29)		47/ /47	41/45	7.9
31111*f*–01101*f*	V	6397.54930 (21)	7046.41558	0.38824313 (49)	0.9146 (21)		48/ /50	45/47	7.4
11121*e*–00001		6515.12063 (30)	6515.50483	0.38420072 (81)	1.2330 (36)		28/ /48	37/39	9.9
11121*f*–00001		6515.12029 (34)	6515.50526	0.3849670 (10)	1.2223 (54)		/46/	22/23	8.2
02231*e*–02201*e*		6710.06944 (26)	8008.86416	0.38287090 (73)	1.3061 (34)		42/ /48	34/42	8.3
02231*f*–02201*f*		6710.07071 (22)	8008.86544	0.38286783 (67)	1.3609 (36)		45/ /35	28/37	5.8
01131*e*–01101*e*	V	6745.11243 (11)	7393.97228	0.38181955 (23)	1.33541 (83)		59/ /53	49/55	4.3
01131*f*–01101*f*	V	6745.112289 (78)	7393.97272	0.38239850 (14)	1.35323 (44)		60/ /48	49/53	2.9
00031–00001	V	6780.210893 (77)	6780.21089	0.38135153 (11)	1.32238 (27)		10/ /68	64/69	3.3
40013–00001[c]	V	7481.57400 (37)	7481.57400	0.3852885 (33)	−1.6882 (66)	−826 (36)	44/ /46	35/45	9.2
40012–00001	V	7600.12116 (19)	7600.12116	0.38587618 (48)	0.8072 (22)		46/ /48	46/48	6.7
11132*e*–01101*e*	V	7929.9100 (11)	8578.77043	0.3824275 (42)	1.405 (32)		35/ /35	23/28	15.2
11132*f*–01101*f*	V	7929.90744 (72)	8578.76888	0.3833988 (34)	1.585 (32)		32/ /34	27/31	15.4
10032–00001	V	7981.18048 (12)	7981.18048	0.38827873 (23)	1.55786 (80)		54/ /56	53/56	4.6
11131*e*–01101*e*	V	8070.91533 (32)	8719.77463	0.3812719 (11)	1.2202 (65)		43/ /41	33/39	8.8
11131*f*–01101*f*	V	8070.91521 (35)	8719.77524	0.3819953 (12)	1.2425 (74)		42/ /42	31/42	9.6
10031–00001	V	8089.021247 (88)	8089.02125	0.38063913 (18)	1.19141 (64)		58/ /58	54/59	3.4

Notes. The uncertainties are given in parentheses in the unit of the last quoted digit. The uncertainty for G_v is the same as that for υ_0 and then not repeated. The label V in the first column indicates that the corresponding band was observed in the spectrum of Venus atmosphere [2]. The parameters for the ground level were taken from [31]. The band origin, υ_0, was obtained from the variation of the vibrational term values: $\upsilon_0 = G'_v - G''_v + B''_v k''^2 - B'_v k'^2$.

[a] n, number of transitions included in the fit; N, number of assigned rotational transitions.

[b] Several weak Q branch lines have been assigned but are not included in the final fitting because they are blended.

[c] Bands affected by perturbations for high J values.

[d] A perturbation has been found near $J' = 32$ and 36 for the e and f component, respectively. Extra lines can be observed.

3.3. $^{18}O^{13}C^{16}O$

A previous contribution has been devoted to the analysis of the transitions of the $^{16}O^{13}C^{18}O$ isotopomer identified in the FTS spectrum [33]. Fourteen bands were detected between 4000 and 9500 cm^{-1}. These results together with the data collected in the literature have allowed the derivation of the corresponding effective Hamiltonian. We then present in Table 6, only the results retrieved from the cw-CRDS spectrum between

Table 3
Spectroscopic parameters (in cm^{-1}) of $^{13}C^{16}O_2$ bands obtained from the analysis of the cw-CRDS spectrum between 6130 and 6750 cm^{-1}

$^{13}C^{16}O_2$		υ_0	G_v	B_v	$D_v \times 10^7$	J_{max} $P/Q/R$	n/N[a]	RMS $\times 10^4$
30013–00001[b]	**V**	**6119.62090 (24)**	**6119.62090**	**0.38758621 (40)**	**1.7579 (12)**	**60/ /76**	**60/68**	**9.7**
22212*e*–00001		6155.41333 (83)	6156.96742	0.3885232 (10)	1.3312 (27)	30/ /58	22/22	9.4
41113*e*–11102*e*		6214.84425 (36)	8111.76849	0.38625037 (86)	1.4546 (38)	47/ /49	33/35	10.3
41113*f*–11102*f*		6214.84393 (33)	8111.76985	0.38793213 (89)	1.5510 (44)	44/ /46	40/40	10.9
40013–10002[b]		6215.7429 (13)	7481.57068	0.3853500 (68)	−0.214 (63)	60/ /62	27/53	40.1
40012–10001		6230.06025 (49)	7600.12236	0.38587410 (74)	0.8011 (21)	64/ /60	56/58	19.2
41112*e*–11101*e*		6230.51642 (56)	8267.99582	0.3860615 (15)	1.0503 (72)	47/ /25	26/27	15.1
41112*f*–11101*f*		6230.51585 (60)	8267.99684	0.3876505 (11)	1.0246 (40)	56/ /44	31/36	15.6
30012–00001[b]	**V**	**6241.96842 (16)**	**6241.96842**	**0.38585833 (22)**	**1.10519 (51)**	**78/ /78**	**68/79**	**7.1**
33311*e*–03301*e*		6442.8422 (13)	8392.70527	0.3903421 (60)	2.193 (51)	33/ /37	23/29	24.7
33311*f*–03301*f*		6442.84848 (77)	8392.71101	0.3902857 (26)	0.850 (16)	32/ /42	28/28	22.3
32212e – 02201*e*[c]		6243.25586 (69)	7542.07100	0.3879789 (13)	1.4529 (40)	52/ /58	38/41	22.9
32212*f*–02201*f*[c]		6243.25782 (54)	7542.06951	0.38796916 (99)	1.2964 (32)	53/ /57	49/49	19.3
31112*e*–01101*e*[c]	**V**	**6243.57308 (30)**	**6892.43752**	**0.38640489 (40)**	**1.25501 (93)**	**69/ /67**	**57/64**	**12.6**
31112*f*–01101*f*[c]	**V**	**6243.57343 (35)**	**6892.43920**	**0.38773101 (44)**	**1.25325 (10)**	**68/ /70**	**54/63**	**13.6**
41101*e*–00001		**6257.02027 (65)**	**6257.40964**	**0.3893692 (14)**	**1.0886 (39)**	**52/ /58**	**40/43**	**17.4**
21123*e*–10002		6297.4759 (18)	6297.86177	0.385824 (16)	1.59 (27)	24/ /22	12/14	22.6
21123*f*–10002						/24/	0/7	
22211*e*–00001		6326.03643 (68)	6327.58891	0.3881190 (82)	1.3700 (20)	62/ /62	38/39	13.1
40012–10002		6334.29287 (51)	7600.12065	0.3858796 (12)	0.8279 (47)	54/ /48	44/45	19.4
12222*e*–01101*e*		6338.42321 (41)	6988.44866	0.3868552 (35)	−16.178 (52)	23/ /33	13/19	7.9
12222*e*–01101*f*		6338.4246 (12)	6988.44982	0.386808 (18)	−17.69 (53)	/18/	9/9	16.5
12222*f*–01101*e*		6338.4246 (16)	6988.44991	0.386813 (16)	−17.20 (29)	/23/	9/9	23.2
12222*f*–01101*f*		6338.4233 (10)	6988.44870	0.3868401 (96)	−16.583 (19)	26/ /28	12/15	12.9
30011–00001[b]	**V**	**6363.62105 (14)**	**6363.62105**	**0.38702817 (38)**	**0.8713 (18)**	**70/ /70**	**48/71**	**5.2**
41112*e*–11102*e*		6371.07183 (67)	8267.99587	0.3860572 (35)	1.019 (28)	37/ /31	13/15	13.8
41112*f*–11102*f*		6371.06853 (75)	8267.99418	0.3876574 (20)	1.0954 (93)	40/ /46	21/23	17.2
11122*e*–00001		6374.50240 (42)	6374.88769	0.3852872 (15)	1.3732 (98)	28/ /68	32/46	12.9
11122*f*–00001		6374.50306 (40)	6374.88933	0.38626717 (83)	1.5494 (32)	/52/	23/24	10.0
40011–10001		6379.02032 (51)	7749.08243	0.38756125 (92)	0.5827 (31)	56/56/	49/50	18.1
31111*e*–01101*e*[c]	**V**	**6397.55053 (31)**	**7046.41540**	**0.38683998 (40)**	**0.96861 (94)**	**63/ /69**	**57/60**	**13.1**
31111*f*–01101*f*[c]	**V**	**6397.54956 (18)**	**7046.41584**	**0.38824234 (24)**	**0.91385 (53)**	**66/ /70**	**60/64**	**7.7**
41111*e*–11101*e*[d]		6402.0977 (16)	8439.57591	0.384912 (22)	2.05 (60)	19/ /25	12/15	21.6
41111*f*–11101*f*		6402.09426 (53)	8439.57632	0.3887177 (14)	0.7550 (61)	26/ /48	26/28	14.1
32211*e*–02201*e*[c,d]		6422.85601 (48)	7721. 67163	0.3880918 (37)	3.628 (57)	44/ /44	22/36	9.4
32211*f*–02201*f*[c,d]		6422.85484 (88)	7721.67050	0.3881007 (38)	2.496 (31)	47/ /53	30/43	23.3
20022*e*–01101*e*		6457.92724 (79)	7106.40527	0.3839944 (15)	1.4806 (51)	23/ /55	30/32	21.7
20022*e*–01101*f*		6457.92740 (61)	7106.40543	0.3840030 (20)	1.502 (12)	/42/	19/19	14.3
21122*e*–10002[b]		6461.1259 (25)	7727.33806	0.384416 (16)	−0.0094 (20)	/ /38	11/18	31.9
21122*f*–10002[b]		6461.1331 (14)	7727.34643	0.3855663 (62)	−0.069 (52)	/42/	13/15	22.3
40011–10002		6483.25464 (51)	7749.08242	0.3875681 (12)	0.6147 (49)	50/ /52	46/46	19.3
13321*e*–02201*e*		6494.29258 (43)	7795.03131	0.3861628 (16)	1.2649 (89)	18/ /42	21/21	11.6
13321*e*–02201*f*		6494.28922 (91)	7795.02809	0.3861792 (25)	1.377 (17)	/39/	15/16	13.1
13321*f*–02201*e*		6494.28969 (91)	7795.02848	0.3861705 (25)	1.298 (14)	/40/	11/13	11.3
13321*f*–02201*f*		6494.29248 (33)	7795.03121	0.3861643 (12)	1.2705 (73)	19/ /39	16/16	6.5
12221*e*–01101*e*		6505.77662 (35)	7155.79617	0.38537893 (70)	1.2771 (24)	39/ /55	43/43	12.3
12221*e*–01101*f*		6505.77713 (40)	7155.79668	0.38537974 (75)	1.2799 (27)	/54/	22/23	9.2
12221*f*–01101*e*		6505.77778 (45)	7155.79731	0.38537638 (79)	1.2568 (25)	/57/	24/24	10.6
12221*f*–01101*f*		6505.77689 (28)	7155.79643	0.38537619 (49)	1.2520 (15)	40/ /58	40/41	9.3
11121*e*–00001		**6515.12076 (21)**	**6515.50496**	**0.38420108 (26)**	**1.23723 (55)**	**52/ /72**	**63/63**	**9.6**
11121*f*–00001		**6515.12029 (30)**	**6515.50526**	**0.38496600 (39)**	**1.21476 (90)**	**/68/**	**32/32**	**9.1**
20021*e*–01101*e*		6560.70060 (19)	7209.17862	0.38369522 (44)	0.9664 (18)	41/ /59	44/47	7.5
20021*e*–01101*f*		6560.70071 (52)	7209.17874	0.3836947 (11)	0.9634 (43)	/52/	26/26	13.6
10032–10001		6611.11871 (25)	7981.18082	0.38227794 (59)	1.5636 (25)	50/ /52	44/46	9.5
03331*e*–03301*e*		6675.08199 (56)	8624.88464	0.3836298 (10)	1.3522 (34)	57/ /47	39/43	16.4
03331*f*–03301*f*		6675.08238 (49)	8624.88503	0.38362996 (95)	1.3536 (33)	56/ /48	42/45	15.1
11132*e*–11102*e*		6681.84783 (46)	8578.76825	0.3824297 (10)	1.4295 (38)	55/ /49	45/47	16.5
11132*f*–11102*f*		6681.84717 (52)	8578.76856	0.38339434 (93)	1.5489 (30)	60/ /46	38/39	17.0
11131*e*–11101*e*		6682.29738 (51)	8719.77199	0.3812743 (14)	1.2359 (62)	49/ /43	26/28	13.1
11131*f*–11101*f*		6682.29710 (68)	8719.77244	0.3819962 (17)	1.2306 (82)	48/ /34	25/25	17.0
00041–00011		6710.02024 (54)	8993.50735	0.3783935 (19)	1.324 (12)	35/ /39	19/19	9.8
02231*e*–02201*e*[c]		**6710.07006 (35)**	**8008.86479**	**0.38286811 (46)**	**1.2910 (11)**	**68/ /58**	**54/58**	**12.4**

Table 3 (*continued*)

$^{13}C^{16}O_2$		υ_0	G_v	B_v	$D_v \times 10^7$	J_{max} $P/Q/R$	n/N[a]	RMS $\times 10^4$
02231*f*–02201*f*[c]		**6710.07059 (45)**	**8008.86532**	**0.38286843 (39)**	**1.36820 (98)**	**67/ /51**	**50/52**	**10.0**
10032–10002		6715.35219 (38)	7981.17997	0.38227807 (51)	1.5622 (13)	70/ /62	52/55	14.4
10031–10001		6718.95835 (30)	8089.02046	0.38073836 (45)	1.1952 (12)	66/ /54	52/53	11.6
01131*e*–01101*e*[c]	**V**	**6745.11237 (19)**	**7393.97222**	**0.38181986 (25)**	**1.33707 (57)**	**73/ /53**	**54/60**	**8.3**
01131*f*–01101*f*[c]	**V**	**6745.11238 (19)**	**7393.97282**	**0.38239830 (22)**	**1.35293 (44)**	**76/ /48**	**57/61**	**8.0**
00031–00001	**V**	**6780.210828 (69)**	**6780.21083**	**0.381351724 (88)**	**1.32301 (20)**	**68/ /72**	**67/70**	**3.1**

Notes. The uncertainties are given in parentheses in the unit of the last quoted digit. The uncertainty for G_v is the same as that for υ_0 and then not repeated. The parameters in bold characters correspond to the bands also observed in our FT spectrum (Table 2), the label V in the first column indicates that the corresponding band was observed in the spectrum of Venus atmosphere [2]. The parameters for the ground level were taken from [31]. The band origin, υ_0, was obtained from the variation of the vibrational term values: $\upsilon_0 = G'_v - G''_v + B''_v k''^2 - B'_v k'^2$.

[a] n, number of transitions included in the fit; N, number of assigned rotational transitions.

[b] Bands affected by perturbations for high J values.

[c] In these Π–Π and Δ–Δ transitions, several weak Q lines have been assigned but not included in the final fitting because they are blended.

[d] Bands in Coriolis interaction responsible of an intensity transfer to extra lines which were observed (see Text and Supplementary Material).

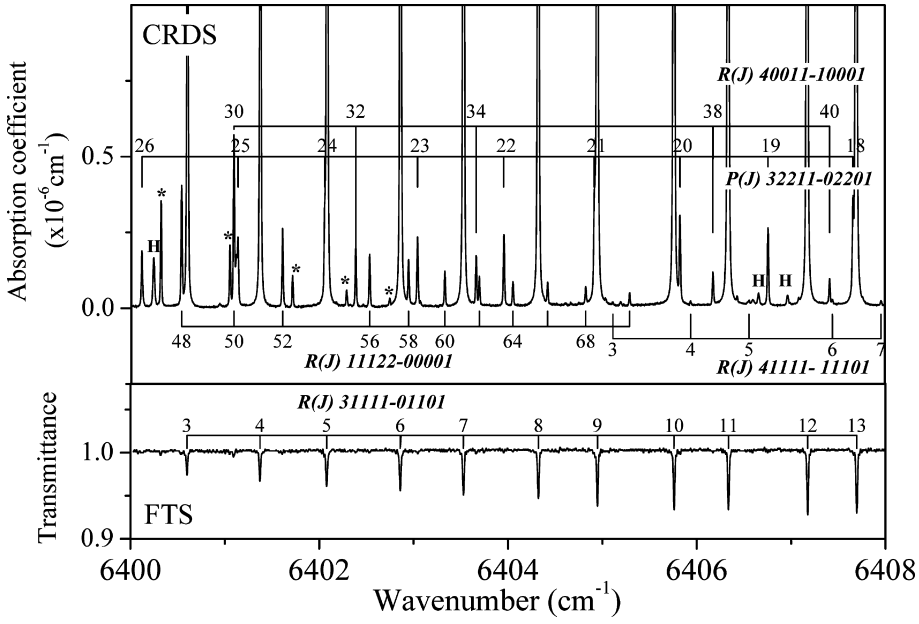

Fig. 4. Comparison of the CRDS and FTS spectra between 6400 and 6408 cm^{-1}. Lines marked by 'H' are water lines. Lines marked by '*' are the $R(62)$–$R(70)$ transitions of the 30011–00001 band.

6100 and 6750 cm^{-1}: five cold bands and eight hot bands could be detected and analysed while only three cold bands (one of them previously observed in Venus spectra [2]) were observed in this spectral region by FTS [33].

There are still a significant number of lines (about 20%) remaining unassigned in the cw-CRDS spectrum. Some of them are not among the weakest and may be due to other isotopomers.

4. Discussion

We present in Table 7 a comparison of the amount of newly observed data with that previously available in HITRAN [1] and in Venus spectra [2] for both CRDS and FTS regions. This table shows in particular that, compared to HITRAN, in the CRDS region, the number of observed lines and bands have been multiplied by about 10 and 7, respectively, and by about 3 and 2 in the FT region.

The Venus bands reported by Mandin [2] allowed a comparison with the FT results. The overall agreement is good but a careful comparison shows a systematic shift on the line positions: in the region between 4600 and 5100 cm^{-1}, our values agree within 0.001–0.002 cm^{-1} with Mandin's values but they are typically 0.003–0.004 cm^{-1} below in the region around 6000–6800 and 0.005–0.006 cm^{-1} below in the region around 7450–8100 cm^{-1}. This shift has then the tendency to increase with the wavenumber. This observation is consistent with the shift in the same direction and with a larger amplitude (0.013 cm^{-1}) that we evidenced in our ICLAS

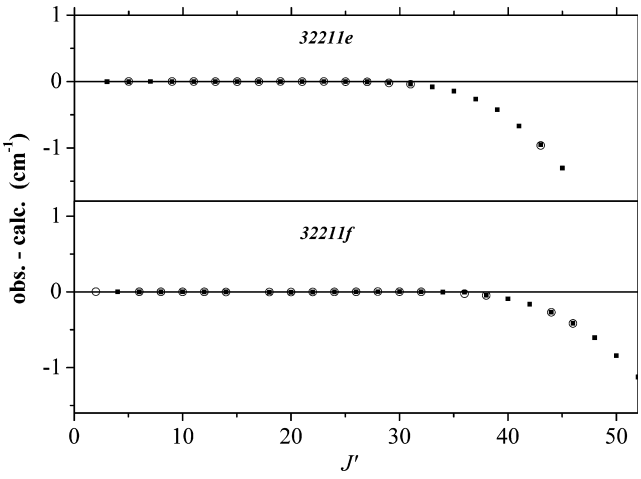

Fig. 5. Plot of the energy difference in the 32211 upper state, between the energies retrieved from the observed lines of the 32211–02201 band centered at 7720.12 cm^{-1} and those of unperturbed levels obtained from the parameters listed in Table 3. For each J' value, the observed energy level of the upper states were obtained from $P(J'+1)$ transitions (open circle) and $R(J'-1)$ transitions (black square).

spectra in the region of the $2\nu_1+3\nu_3$ triad near 9500 cm^{-1} [4]. The good agreement observed in the 4000–5000 cm^{-1} region is not fortuitous as CO lines in this region were used to correct the Doppler shift affecting Venus data [2]. The slow increase of the deviations is then probably due to a residual in the Doppler correction of Venus data at high energy. These deviations are satisfactorily corrected by the calibration factor obtained for Venus data from the simultaneous analysis of all observed line positions with the help of Ritz principle (see below). It should be emphasized that the addition of new measured data does not change considerably the calibration factor previously determined [7].

The comparison of all measured data to HITRAN data shows a rather good agreement except for a few bands. As illustrated in Fig. 6 in the case of the 30012–00001 band, the residuals are usually within a few thousandth of cm^{-1}. In Fig. 7, we present the average deviation of the different $^{13}C^{16}O_2$ bands listed in HITRAN compared to our FTS values. In the case of the 30013–00001 band the residuals increase with J and reach the value of 0.030 cm^{-1} at $J=59$ (see Fig. 8). Much higher discrepancies are observed for the 31112–01101 hot band (Fig. 9): for the f component the deviation is about -0.090 cm^{-1} while for the e component it increases from -0.092 cm^{-1} at $J=6$ to -0.524 cm^{-1} at $J=31$. Note that Figs. 7–9 clearly show the increased accuracy of our measurements compared to Venus data.

5. Global fitting of the $^{13}C^{16}O_2$ line positions

The present results have confirmed the very good predictive abilities of the set of effective Hamiltonian parameters published in our previous contribution [7] for the $^{13}C^{16}O_2$ species: typical residuals between the observed and predicted line positions are of the order of a few of thousandth of cm^{-1}. We, however, decided to perform a new global fitting of the line positions of this isotopomer by adding the present data and recent mea-

Table 4
Spectroscopic parameters (in cm^{-1}) of the $^{16}O^{13}C^{17}O$ bands obtained from the analysis of the FT spectrum between 4000 and 8500 cm^{-1}

$^{16}O^{13}C^{17}O$	υ_0	B_v	$D_v \times 10^7$	J_{max} $P/Q/R$	n/N[a]	RMS $\times 10^4$
00021–00001 V	4524.88113 (17)	0.37287618 (60)	1.2510 (41)	37/ /40	61/69	6.0
20013–00001 V	4719.11870 (19)	0.37709038 (53)	1.7045 (27)	46/ /44	75/79	7.9
20012–00001	4849.39270 (12)	0.37523329 (25)	1.34907 (95)	54/ /54	94/97	6.0
20011–00001	4955.59042 (11)	0.37554895 (27)	0.8915 (12)	47/ /59	81/84	5.3
30012–00001	6188.05233 (30)	0.3745890 (13)	0.9440 (98)	39/ /39	60/73	11.0
00031–00001	6752.41245 (41)	0.3700044 (15)	1.2325 (94)	40/ /41	63/70	15.7

Notes. The uncertainties are given in parentheses in the unit of the last quoted digit. The label V in the first column indicates that the corresponding band was observed in the spectrum of Venus atmosphere [2]. The parameters for the ground level were taken from [31].

[a] n, number of transitions included in the fit; N, number of assigned rotational transitions.

Table 5
Spectroscopic parameters (in cm^{-1}) of the $^{16}O^{13}C^{17}O$ bands obtained from the analysis of the cw-CRDS spectrum between 6130 and 6750 cm^{-1}

$^{16}O^{13}C^{17}O$	υ_0	B_v	$D_v \times 10^7$	J_{max} $P/Q/R$	n/N[a]	RMS $\times 10^4$
30012–00001	**6188.05219 (21)**	**0.37458542 (46)**	**0.9721 (18)**	**54/ /54**	**94/102**	**10.7**
30011–00001	6318.43392 (28)	0.37592819 (58)	0.7013 (21)	51/ /55	94/96	14.8
00031–00001	**6752.41226 (25)**	**0.36999871 (87)**	**1.2284 (57)**	**40/ /41**	**64/68**	**9.5**

Note. The uncertainties are given in parentheses in the unit of the last quoted digit. The parameters in bold characters correspond to the bands also observed in the FT spectrum (Table 4). The parameters for the ground level were taken from [31].

[a] n, number of transitions included in the fit; N, number of assigned rotational transitions.

Table 6
Spectroscopic parameters (in cm^{-1}) of $^{16}O^{13}C^{18}O$ transitions obtained from the analysis of the cw-CRDS spectrum between 6130 and 6750 cm^{-1}

$^{16}O^{13}C^{18}O$	v_0	G_v	B_v	$D_v \times 10^7$	J_{max} $P/Q/R$	n/N[a]	RMS $\times 10^4$
40012–10001	6136.34488 (58)	7478.62266	0.3648839 (20)	1.071 (13)	8/ /41	28/29	16.1
30012–00001	**6140.12350 (27)**	**6140.12350**	**0.36452905 (53)**	**0.8625 (19)**	**45/ /56**	**95/96**	**14.1**
31112*e*–01101*e*	6146.94934 (20)	6790.64323	0.36489311 (48)	1.0660 (18)	19/ /55	58/60	9.6
31112*f*–01101*f*	6146.94880 (17)	6790.64392	0.36612231 (38)	1.0353 (15)	21/ /55	59/64	7.6
32212–02201[b]	6149.25669 (74)	7437.70390	0.3663042 (49)	1.023 (573	22/ /29	26/27	18.5
30011–00001	**6279.48827 (29)**	**6279.48827**	**0.36591331 (60)**	**0.6649 (21)**	**36/ /56**	**80/82**	**14.6**
31111*e*–01101*e*	6311.98845 (32)	6955.68303	0.36558302 (73)	0.8868 (30)	45/ /51	74/77	14.4
31111*f*–01101*f*	6311.98721 (40)	6955.68318	0.3669781 (13)	0.8395 (72)	41/ /43	71/72	17.6
11122*e*–00001	6314.55654 (51)	6314.91988	0.3633377 (27)	1.316 (23)	20/ /34	31/34	14.8
11122*f*–00001	6314.55478 (69)	6314.91898	0.3631990 (23)	1.398 (16)	/38/	26/27	13.7
11121*e*–00001	6449.12333 (37)	6449.48606	0.36272792 (88)	1.0788 (35)	29/ /52	74/78	17.4
11121*f*–00001	6449.12647 (33)	6449.48994	0.36347270 (77)	1.0716 (34)	/50/	43/44	10.9
02231–02201[b]	6659.01433 (42)	7947.44133	0.36124962 (99)	1.2016 (45)	56/ /42	70/78	17.2
10032–10002	6666.66778 (38)	7911.56801	0.36043252 (90)	1.3832 (38)	53/ /37	69/70	17.0
10031–10001	6666.97498 (54)	8009.25276	0.3595236 (13)	0.9974 (60)	50/ /37	42/47	16.2
01131*e*–01101*e*[c]	6693.65654 (40)	7337.34582	0.36027852 (51)	1.1925 (12)	67/ /59	64/96	13.6
01131*f*–01101*f*[c]	6693.65558 (41)	7337.34536	0.36078436 (48)	1.1948 (11)	68/ /56	65/97	14.3
00031–00001 V	**6728.35488 (12)**	**6728.35488**	**0.35981584 (16)**	**1.17516 (34)**	**73/ /68**	**121/130**	**7.5**

Notes. The uncertainties are given in parentheses in the unit of the last quoted digit. The uncertainty for G_v is the same as that for v_0 and then not repeated. The parameters in bold characters correspond to the bands also observed in the present FT spectrum and recently published in a separate contribution [33]. The label V in the first column indicates that the corresponding band was observed in the spectrum of Venus atmosphere [2]. The parameters of the ground level were taken from [31]. The band origin, v_0, was obtained from the variation of the vibrational term values: $v_0 = G'_v - G''_v + B''_v k''^2 - B'_v k'^2$.

[a] n, number of transitions included in the fit; N, number of assigned rotational transitions.

[b] The e and f component of the 32212–02201 and 02231–02201 hot bands are blended leading to a single set of parameters for both components.

[c] In the R branch, transitions corresponding to the e and f components are overlapping and then not included in the fit.

Table 7
Comparison of the number of line positions and bands observed for the $^{13}C^{16}O_2$, $^{16}O^{13}C^{17}O$, and $^{16}O^{13}C^{18}O$ isotopic species

		HITRAN	Venus	FTS	cw-CRDS
cw-CRDS spectral region: 6130 and 6750 cm^{-1}					
Bands	$^{13}C^{16}O_2$	6	7	10	39
	$^{16}O^{13}C^{17}O$	0	0	2	3
	$^{16}O^{13}C^{18}O$	0	1	3	13
	Total	6	8	15	55
Lines	Total	232	275	948	4018
FTS spectral region: 4400 and 8500 cm^{-1}					
Bands	$^{13}C^{16}O_2$	22	27	36	
	$^{16}O^{13}C^{17}O$	0	2	6	
	$^{16}O^{13}C^{18}O$	3	6	14[a]	
	Total	25	35	56	
Lines	Total	1393	1303	4277	

[a] Ref. [33].

surements above 10 000 cm^{-1} [5], to the data set previously considered [8–28]. Indeed, this new fit is suitable for two reasons. First, the new data obtained in this work represent an important extension and improvement of the available data set (see Table 7): 3870 new line positions have been determined compared to 10 865 included in our previous fit [7]. Second, several bands show significant residuals which can reach 0.015 cm^{-1} and, in the particular case of the 41111–11101 and 30022–11101 bands, which are in resonance Coriolis interaction, the deviations reach a value of 0.030 cm^{-1}.

The same polyad model of effective Hamiltonian as in our previous papers [7,35] was used. Before fitting, the consistency of all collected data was checked with the help of Ritz principle. This procedure which is described, for example, in [33], allows one to detect outliers, i.e., misprints, misassignments, and to account for possible calibration factors.

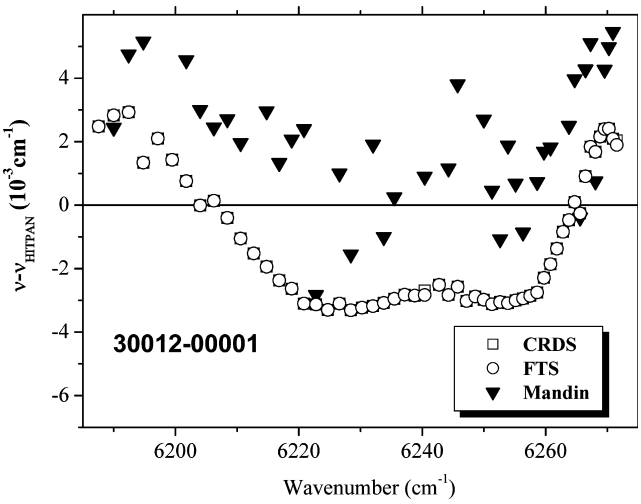

Fig. 6. Residuals between measured (CRDS, FTS, and Venus) line positions and those presented in HITRAN database for the 30012–00001 band of $^{13}C^{16}O_2$.

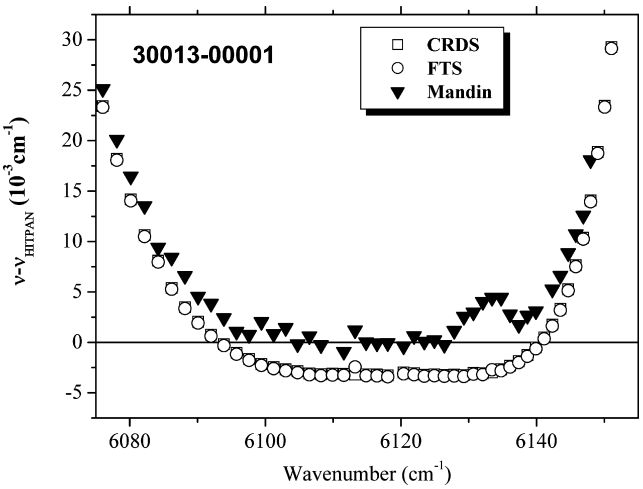

Fig. 8. Residuals between measured (CRDS, FTS, and Venus) line positions and those presented in HITRAN database for the 30013–00001 band $^{13}C^{16}O_2$.

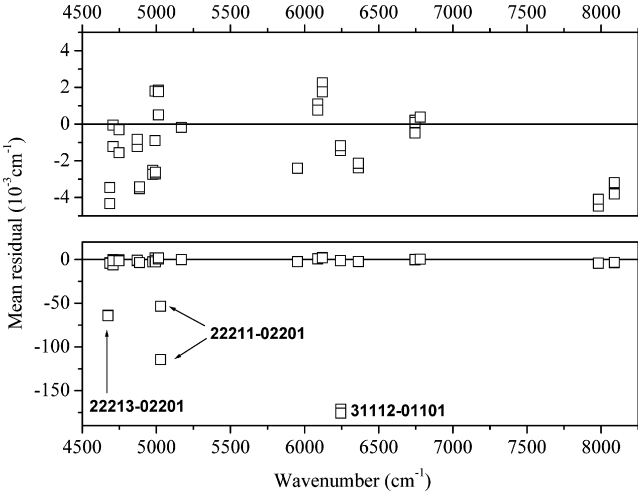

Fig. 7. Average differences between the FTS and HITRAN line positions for the $^{13}C^{16}O_2$ bands listed in HITRAN between 4500 and 8250 cm^{-1} as a function of the band centers. The ordinate scale of the upper panel is enlarged by a factor 20 compared to that of the lower panel.

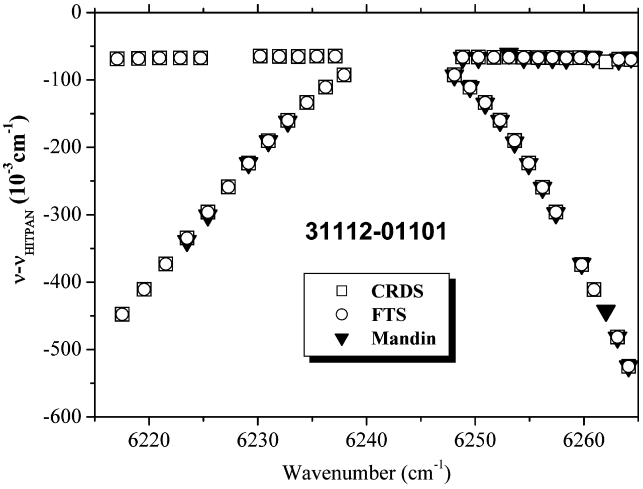

Fig. 9. Residuals between measured (CRDS, FTS, and Venus) line positions and those presented in HITRAN database for the 31112–01101 band $^{13}C^{16}O_2$.

The source-by-source characteristics of the input data are given in Table 8. They include, for each source, the calibration factors, experimental uncertainties, and root mean squares of residuals defined according to the following equation:

$$\mathrm{RMS_{RITZ}} = \sqrt{\frac{1}{N_{\mathrm{tra}}}\sum[(1+\delta^k)\nu^k_{j\leftarrow i} - E_j + E_i]^2}, \qquad (3)$$

where $(1+\delta^k)$ is the calibration factor for the kth experimental source, E_j and E_i are energies of upper and lower states, respectively, $\nu^k_{j\leftarrow i}$ is the wavenumber of the transition between these states, and N_{tra} is the number of transitions belonging to the kth source. The energies E_j and E_i and calibration factors $(1+\delta^k)$ have been determined by applying the Ritz computer code to the collected set of observed line positions. The values of the calibration offsets δ^k were fixed to zero for the laser heterodyne measurements [8–10]. The values of $\mathrm{RMS_{RITZ}}$ can be considered as the actual average experimental precision of the data. The calibration factors presented in Table 8 have been obtained from a global Ritz analysis including the measured line positions for all isotopic species of carbon dioxide. As a result of recent measurements from a number of new experimental sources, some of these calibration factors slightly differ from those listed in Table 2 of [7]. This use of the Ritz procedure [33] insures the consistency between all

Table 8
Experimental data and statistics of the line positions fit for $^{13}C^{16}O_2$

Reference	Calibration factor	Precision (in 10^{-3} cm^{-1})	N_{fit}	RMS_{RITZ} (in 10^{-3} cm^{-1})	RMS_{GIP} (in 10^{-3} cm^{-1})
Maki et al. [8]	1.000000000[a]	0.00033	92	<0.0001	<0.0001
Freed et al. [9]	1.000000000[a]	0.001	86	0.0002	<0.0001
Petersen et al. [10]	1.000000000[a]	0.033	31	0.016	0.091
Jolma [11]	1.000000000	0.04[c]	447	0.035	0.14
Siemsen [12]	1.000000000	0.04	41	0.02	0.08
Kauppinen et al. [13,14]	0.999999911	0.04	41	0.04	0.08
Malathy Devi et al. [15]	0.999999957	0.10	110	0.09	0.13
Guelachvili [16]	0.999999806	0.12	106	0.10	0.17
Rinsland et al. [17]	1.000000085	0.50[c]	93	0.33	0.44
Rinsland et al. [18]	1.000000058	0.50[c]	48	0.44	0.58
Rinsland et al. [19]	1.000000074	0.50[c]	72	0.43	0.70
Benner et al. [20]	1.000000750	0.50[c]	27	0.43	0.74
Bailly [21]	0.999999678	0.50[c]	1020	0.25	1.46
Bailly et al. [22]	0.999999773	0.50[c]	205	0.15	0.32
Esplin et al. [23]	0.999999881	0.40	1320	0.34	1.20
Esplin et al. [24]	1.000000895	1.00	39	0.46	0.98
Esplin et al. [25]	1.000000000	0.50	4417	0.46	0.85
Paso et al. [26]	0.999998948	0.80	64	0.68	0.68
Mandin, Venus [2]	0.999999386	2.00[c]	982	1.61	2.33
Mandin, Mars [2]	0.999999697	2.00[c]	88	1.11	2.28
Baldacci et al. [27]	0.999999812	3.00	664	2.46	2.82
Baldacci et al. [28]	1.000000081	5.00	1195	3.78	4.72
Tashkun et al. [7]	1.000000000[b]	5.00	59	2.80	7.87
Weirauch et al. [5]	1.000000000[b]	5.00	90	3.15	6.03
This work, FTS	0.999999965	1.00	2097	0.41	1.01
This work, CRDS	1.000000000	2.00	1773	1.27	2.89

Spectrum-by-spectrum analysis.
[a] Fixed value.
[b] Could not be determined.
[c] Experimental precision is set to a guessed value N_{fit} is the number of lines included in the fit.

data and all experimental sources in the least-squares sense.

The least-squares fit of the effective Hamiltonian parameters to the observed line positions has been performed with the help of the GIP computer code [36]. The aim of the fitting procedure was to minimize the dimensionless weighted standard deviation defined according to the usual formula

$$\chi_{GIP} = \sqrt{\frac{\sum_i [(\nu_i^{obs} - \nu_i^{calc})/\varepsilon^k]^2}{N-n}}, \quad (4)$$

where N is the number of fitted transitions, n is the number of adjusted parameters, and ε^k is the experimental uncertainty of the kth spectrum. The values given in column 3 (“Precision”) of Table 8 were used in the fit as experimental uncertainties. The values of the parameters previously published [7] were used as initial guess.

More than 14 650 line positions of 181 bands were used to fit 96 parameters of the effective Hamiltonian (see Table 9). The dimensionless weighted standard deviation is $\chi = 2.00$ while the RMS of the fit is 0.002 cm^{-1}. In Table 8 the RMS_{GIP} are presented for each experimental source. These values are close to the RMS_{RITZ} indicating that the effective Hamiltonian model is adequate to data in a sense that it can reproduce the observed line positions with the accuracy close to the experimental uncertainties. The fit statistics for each band is presented in Table 10. In this table only the newly observed bands are listed as for the other bands, the statistics is not considerably modified compared to that presented in Table 1 of [7].

6. Conclusion

This work represents the first spectroscopic application of the fibered cw-CRDS setup based on DFB lasers, developed in Grenoble. The performances of this spectrometer make it an ideal tool for high sensitivity spectroscopy in the near infrared. In particular, the use of fibered diode lasers makes it easy to change wavelength on an interval covering the whole long-distance telecommunication range (1480–1630 nm). We plan to acquire a single set of mirrors centered on this range to improve still the data collection efficiency (down to about 1 day for the whole range, at full resolution). A quick comparison with multipass absorption coupled with FTS, can be done by considering the following parameters for the two setups: detection limit (noise-equivalent absorption coefficient),

Table 9
The effective Hamiltonian parameters for $^{13}C^{16}O_2$

N	Parameter	Value (cm^{-1})	Order
Diagonal vibrational parameters			
1	ω_1	1353.6230(21)	
2	ω_2	653.72419(54)	
3	ω_3	2328.02837(50)	
4	x_{11}	−2.9036(14)	
5	x_{12}	−3.93332(50)	
6	x_{13}	−18.6336(14)	
7	x_{22}	1.234433(58)	
8	x_{23}	−11.75615(20)	
9	x_{33}	−11.754441(16)	
10	$x_{\ell\ell}$[a]	−0.6764440306	
11	y_{111}	−0.176(32)	10^{-2}
12	y_{112}	−1.86(14)	10^{-2}
13	y_{113}	−9.189(88)	10^{-2}
14	y_{122}	−0.94(10)	10^{-2}
15	y_{123}	2.411(66)	10^{-2}
16	y_{133}	2.818(22)	10^{-2}
17	y_{222}	−0.5133(71)	10^{-2}
18	y_{223}	−0.531(16)	10^{-2}
19	y_{233}	0.8474(63)	10^{-2}
20	y_{333}	0.0772(19)	10^{-2}
21	$y_{1\ell\ell}$	0.638(77)	10^{-2}
22	$y_{2\ell\ell}$	0.4532(71)	10^{-2}
23	$y_{3\ell\ell}$	1.127(15)	10^{-2}
24	z_{1112}	11.5(10)	10^{-4}
25	z_{1113}	−12.7(22)	10^{-4}
26	z_{1122}	9.43(67)	10^{-4}
27	z_{1123}	−41.6(15)	10^{-4}
28	z_{1133}	45.9(21)	10^{-4}
29	z_{1223}	−15.62(62)	10^{-4}
30	z_{1233}	26.67(71)	10^{-4}
31	z_{1333}	18.99(34)	10^{-4}
32	z_{2222}	−0.0936(59)	10^{-4}
33	z_{2233}	2.10(11)	10^{-4}
34	z_{2333}	3.727(25)	10^{-4}
35	z_{3333}	2.8124(24)	10^{-4}
Diagonal rotational and vibrational–rotational parameters			
36	B_e	0.391632017(8)	
37	α_1	1.19506(18)	10^{-3}
38	α_2	−0.702285(33)	10^{-3}
39	α_3	2.986757(74)	10^{-3}
40	γ_{11}	0.092(13)	10^{-5}
41	γ_{12}	−1.3643(97)	10^{-5}
42	γ_{13}	−0.795(21)	10^{-5}
43	γ_{22}	−0.40513(95)	10^{-5}
44	γ_{23}	1.2779(81)	10^{-5}
45	γ_{33}	0.0821(23)	10^{-5}
46	ε_{111}	−2.48(28)	10^{-7}
47	ε_{112}	1.31(33)	10^{-7}
48	ε_{113}	−2.98(40)	10^{-7}
49	ε_{122}	0.60(13)	10^{-7}
50	ε_{123}	−7.65(35)	10^{-7}
51	ε_{133}	1.72(29)	10^{-7}
52	ε_{222}	−0.219(10)	10^{-7}
53	ε_{223}	0.760(60)	10^{-7}
54	ε_{233}	1.159(74)	10^{-7}
55	ε_{333}	0.3838(78)	10^{-7}
56	D_e	0.1311486(32)	10^{-6}
57	β_1	0.0597(11)	10^{-9}
58	β_2	2.2264(12)	10^{-9}
59	β_3	−0.2754(18)	10^{-9}
60	H[a]	0.6316510704	10^{-14}
Parameters of ℓ-doubling matrix elements			
61	L_e	−0.157585(12)	10^{-3}
62	L_1	0.462(16)	10^{-5}
63	L_2	− 0.1785(36)	10^{-5}
64	L_3	0.1398(38)	10^{-5}
65	L_{11}	−7.26(69)	10^{-7}
66	L_{12}	−4.09(18)	10^{-7}
67	L_{22}	1.168(82)	10^{-7}
68	L_{23}	−0.749(46)	10^{-7}
69	L_{33}	−0.572(23)	10^{-7}
70	L_J	0.19065(52)	10^{-9}
Parameters of Fermi-interaction matrix elements			
71	F_e	−25.54127(10)	
72	F_1	0.24503(30)	
73	F_2	0.244624(67)	
74	F_3	0.17159(16)	
75	F_{11}	−0.1291(54)	10^{-2}
76	F_{12}	−0.1033(60)	10^{-2}
77	F_{13}	1.0431(72)6	10^{-2}
78	F_{22}	0.0091(13)	10^{-2}
79	F_{23}	0.1019(36)	10^{-2}
80	F_{33}	−0.2505(39)	10^{-2}
81	F_J	0.100311(11)	10^{-3}
82	F_L	−0.7078(19)	10^{-5}
83	F_{L1}	0.342(21)	10^{-6}
84	F_{L2}	−0.2932(87)	10^{-6}
85	F_{L3}	−0.3297(80)	10^{-6}
86	F_{LJ}	−0.414(11)	10^{-10}
87	F_e^{IV}	0.719(22)	10^{-2}
88	F_1^{IV}	−0.119(17)	10^{-3}
89	F_2^{IV}	0.0818(28)	10^{-3}
90	F_3^{IV}	−0.367(14)	10^{-3}
91	F_J^{IV}	−0.555(33)	10^{-7}
92	F_e^{III}	−0.430(13)	
93	F_e^4	0.2253(22)	
Parameters of Coriolis-interaction matrix elements			
94	C_e	−0.2795(20)	10^{-1}
95	C_1	0.3720(84)	10^{-3}
96	C_{e1}	−0.2554(24)	10^{-2}
97	C_{e2}	0.4606(44)	10^{-2}

Notes. Uncertainties in parentheses represent one standard deviation in units of the last quoted digit.

[a] Fixed to the value given in [32].

acquisition time for a given spectral range, sample volume (relevant when using expensive, isotopically substitutes samples). For the present case, the FTS setup achieved a detection limit of about 10^{-7}/cm with a multipass length of 105 m, to be compared with the best value of 3×10^{-10}/cm for the cw-CRDS setup. The acquisition time for CRDS is about 1 cm^{-1}/min, with a total covered range of 600 cm^{-1}. For FTS, it took about 20 h for a range of 5000 cm^{-1}, which gives 4 cm^{-1}/min, for a total covered range almost 10 times larger than in cw-CRDS. It is then clear that FTS is better in terms of spectral coverage and data acquisition rate, which was quite evident beforehand. On the other hand, cw-CRDS wins in terms of sensitivity by a factor 300 compared with a multipass FTS system.

Table 10
Experimental data and statistics of the line positions fit for $^{13}C^{16}O_2$

$P' \rightarrow P$	$V' \rightarrow V$	v_0	J_{max}	N_{lin}	RMS	References
7 0	01121 00001	5168.599	55	86	1.17	a, FTS
9 0	00031 00001	6780.211	69	85	1.25	a, FTS
9 0	11121 00001	6515.120	73	153	1.48	FTS, CRDS
9 0	11122 00001	6374.503	69	69	3.01	CRDS
9 0	30011 00001	6363.621	71	175	1.31	a, FTS, CRDS
9 0	30012 00001	6241.968	69	177	1.37	a, FTS, CRDS
9 0	30013 00001	6119.621	61	166	1.19	a, FTS, CRDS
9 0	30014 00001	5951.602	53	91	1.15	a, FTS
9 0	41101 00001	6257.020	55	70	1.59	FTS, CRDS
9 2	30011 10001	4993.560	51	43	0.58	FTS
9 2	30011 10002	5097.793	41	35	0.81	FTS
9 2	30012 10002	4976.141	51	40	0.94	FTS
9 2	30012 10001	4871.906	55	42	0.90	FTS
9 2	30013 10001	4749.558	45	34	0.71	FTS
9 2	30013 10002	4853.793	53	44	0.88	FTS
10 1	01131 01101	6745.112	77	292	1.09	a, FTS, CRDS
10 1	12221 01101	6505.777	59	131	1.72	CRDS
10 1	12222 01101	6338.423	20	36	1.60	CRDS
10 1	20021 01101	6560.701	54	70	1.06	CRDS
10 1	20022 01101	6457.927	54	49	3.04	CRDS
10 1	31111 01101	6397.550	71	282	1.03	a, FTS, CRDS
10 1	31112 01101	6243.573	70	236	1.11	a, FTS, CRDS
10 1	31113 01101	6088.214	52	145	1.54	a, FTS
10 1	31114 01101	5904.447	39	86	2.10	a, FTS
11 0	10031 00001	8089.021	55	106	1.23	a, FTS
11 0	10032 00001	7981.180	57	101	2.16	a, FTS
11 0	40012 00001	7600.121	49	76	1.48	a, FTS
11 0	40013 00001	7481.574	45	69	1.27	a, FTS
11 2	02231 02201	6710.071	69	179	1.04	FTS, CRDS
11 2	10031 10001	6718.958	67	53	1.72	CRDS
11 2	10032 10001	6611.119	53	44	1.86	CRDS
11 2	10032 10002	6715.352	71	53	1.66	CRDS
11 2	13321 02201	6494.291	43	62	4.56	CRDS
11 2	21122 02201		46	21	4.78	CRDS
11 2	21122 10002	6461.130	39	29	4.35	CRDS
11 2	21123 10002	6297.476	25	14	2.88	CRDS
11 2	32211 02201	6422.855	58	75	2.82	CRDS
11 2	32212 02201	6243.257	59	87	3.02	CRDS
11 2	40011 10002	6483.255	53	46	2.57	CRDS
11 2	40011 10001	6379.020	57	49	3.40	CRDS
11 2	40012 10001	6230.060	65	55	2.35	CRDS
11 2	40012 10002	6334.293	55	43	2.06	CRDS
11 2	40013 10002	6215.743	63	52	2.97	CRDS
11 2	40013 10001		49	5	2.75	CRDS
12 1	11131 01101	8070.915	44	113	1.83	a, FTS
12 1	11132 01101	7929.909	36	65	1.73	a, FTS
12 3	00041 00011	6710.020	40	19	0.98	CRDS
12 3	03331 03301	6675.082	62	85	1.76	CRDS
12 3	11131 11101	6682.297	50	50	2.20	CRDS
12 3	11132 11102	6681.847	61	83	3.36	CRDS
12 3	30022 11101		26	3	3.11	CRDS
12 3	33311 03301	6442.845	43	51	2.99	CRDS
12 3	41111 11101	6402.096	49	50	6.09	CRDS
12 3	41112 11101	6230.516	57	62	2.85	CRDS
12 3	41112 11102	6371.070	38	31	2.84	CRDS
12 3	41113 11102	6214.844	50	74	1.87	CRDS
15 0	30031 00001	10730.982	39	28	5.62	b
15 0	30032 00001	10616.828	41	31	5.14	b
15 0	30033 00001	10491.435	41	31	7.12	b

Band-by-band analysis; P' and P are upper and lower polyad numbers ($P = 2V_1 + V_2 + 3V_3$), V' and V are upper and lower vibrational states according to HITRAN notation, v_0 is the approximate value of the band center in cm^{-1}, J_{max} is the maximum value of the rotational quantum number in the file of experimental data for a given band, N_{lin} is the total number of lines in the file of the experimental data for a given band, RMS (in $10^{-3}\,cm^{-1}$) is the root-mean-square deviation for a given band. References: a—Ref. [2], b—Ref. [5], FTS—this work Fourier transform spectrum, and CRDS—this work cavity ring down spectrum.

The combination of the results obtained by CRDS and FTS has led to a considerable improvement of the knowledge and accuracy of the absorption spectrum of $^{13}CO_2$. In particular, our measurements have shown (i) an overall good agreement with HITRAN [1] and Venus data [2], (ii) a systematic shift of the order of $0.005\,cm^{-1}$, increasing with the energy, of the line positions obtained from the Venus spectrum and (iii) a few important deviations (up to $0.5\,cm^{-1}$) compared with HITRAN.

The good predictive ability of the effective Hamiltonian model has been fully confirmed. However, considering the amount and improved accuracy of the new data together with the evidence of a few significant deviations, we have performed a new global fitting of all available line positions relative to the $^{13}CO_2$ species using the effective Hamiltonian approach. The refined set of 96 effective Hamiltonian parameters reproduces the observed line positions of more than 14 650 lines of $^{13}C^{16}O_2$ with $RMS = 0.002\,cm^{-1}$.

Intensity measurements which are of first importance for atmospheric applications, will be presented in a future contribution. In this context, the FTS and CRDS methods appear highly complementary: the high data acquisition speed of FTS makes this method suitable for recordings over wide spectral regions with different gas pressures while CRDS has the advantage of a much higher sensitivity.

Acknowledgments

This work is jointly supported by CNRS in the frame of the "Programme National de Chimie Atmosphérique," the National Natural Science Foundation of China (20103007, 50121202), the National Project for the Development of Key Fundamental Sciences in China and the Russian Academy of Sciences within the framework of the program 2.10 "Optical Spectroscopy and Frequency Standards." Collaborative projects between CNRS and RFBR (PICS Grant 01-05-22002) and between CNRS and the Chinese Academy of Science (No. 12491) are also acknowledged. The authors are grateful to Drs. D. Bailly, J.-Y. Mandin, and M.P. Esplin for providing them with the files of observed line positions. P.M. acknowledges a financial support by EU (Contract HPRN-CT-2000-00022).

References

[1] L.S. Rothman, A. Barbe, D.C. Benner, L.R. Brown, C. Camy-Peyret, M.R. Carleer, K. Chance, C. Clerbaux, V. Dana, V.M. Devi, A. Fayt, J.-M. Flaud, R.R. Gamache, A. Goldman, D. Jacquemart, K.W. Jucks, W.J. Lafferty, J.-Y. Mandin, S.T. Massie, V. Nemtchinov, D.A. Newnham, A. Perrin, C.P. Rinsland, J. Schroeder, K.M. Smith, M.A.H. Smith, K. Tang, R.A. Toth, J. Vander Auwera, P. Varanasi, K. Yoshino, J. Quant. Spectrosc. Radiat. Transfer 82 (2003) 5–44.

[2] J.-Y. Mandin, J. Mol. Spectrosc. 67 (1977) 304–321.

[3] P. Connes, G. Michel, Astrophys. J. Lett. Ed. 190 (1974) L24.

[4] Y. Ding, E. Bertseva, A. Campargue, J. Mol. Spectrosc. 212 (2002) 219–222.

[5] G. Weirauch, A. Campargue, J. Mol. Spectrosc. 207 (2001) 263–268.

[6] A. Goldman, T.M. Stephen, L.S. Rothman, L.P. Giver, J.-Y. Mandin, R.R. Gamache, C.P. Rinsland, F.J. Murcray, J. Quant. Spectrosc. Radiat. Transfer 82 (2003) 197–205.

[7] S.A. Tashkun, V.I. Perevalov, J.-L. Teffo, M. Lecoutre, T.R. Huet, A. Campargue, D. Bailly, M.P. Esplin, J. Mol. Spectrosc. 200 (2000) 162–176.

[8] A.G. Maki, Che-Chung Chou, K.M. Evenson, L.R. Zink, Jow-Tsong Shy, J. Mol. Spectrosc. 167 (1994) 211–224.

[9] C. Freed, L.C. Bradley, R.G. O'Donnell, IEEE J. Quantum Electron. 16 (1980) 1195–1206.

[10] F.R. Petersen, J.S. Wells, A.G. Maki, K.J. Siemsen, Appl. Opt. 20 (1981) 3635–3640.

[11] K. Jolma, J. Mol. Spectrosc. 111 (1985) 211–218.

[12] K.J. Siemsen, Opt. Commun. 34 (1980) 447–450.

[13] J. Kauppinen, K. Jolma, V.-M. Horneman, Appl. Opt. 21 (1982) 3332–3336.

[14] K. Jolma, J. Kauppinen, V.-M. Horneman, J. Mol. Spectrosc. 101 (1983) 300–305.

[15] V. Malathy Devi, D.C. Benner, M.A.H. Smith, C.P. Rinsland, J. Quant. Spectrosc. Radiat. Transfer 76 (2003) 289–307.

[16] G. Guelachvili, J. Mol. Spectrosc. 79 (1980) 72–83.

[17] C.P. Rinsland, D.C. Benner, Appl. Opt. 23 (1984) 4523–4528.

[18] C.P. Rinsland, D.C. Benner, V. Malathy Devi, Appl.Opt. 24 (1985) 1644–1650.

[19] C.P. Rinsland, D.C. Benner, V. Malathy Devi, Appl. Opt. 25 (1986) 1204–1214.

[20] D.C. Benner, V. Malathy Devi, C.P. Rinsland, P.S. Ferry-Leeper, Appl. Opt. 27 (1988) 1588–1597.

[21] D. Bailly, Thesis, Paris, 1983.

[22] D. Bailly, C. Rossetti, J. Mol. Spectrosc. 105 (1984) 229–245.

[23] M.P. Esplin, L.S. Rothman, J. Mol. Spectrosc. 116 (1986) 351–363.

[24] M.P. Esplin, R.J. Huppi, G.A. Vanasse, Appl. Opt. 21 (1982) 1681–1685.

[25] M.P. Esplin, M.L. Hoke, in: High Resolution Fourier Transform Spectroscopy Technical Digest, vol. 21, OSA, Washington, DC, 1992, pp. 78–80.

[26] R. Paso, J. Kauppinen, R. Anttila, J. Mol. Spectrosc. 79 (1980) 236–253.

[27] A. Baldacci, L. Linden, V. Malathy Devi, K.N. Rao, B. Fridovich, J. Mol. Spectrosc. 72 (1978) 135–142.

[28] A. Baldacci, C.P. Rinsland, M.A.H. Smith, K.N. Rao, J. Mol. Spectrosc. 94 (1982) 351–362.

[29] D. Romanini, A.A. Kachanov, N. Sadeghi, F. Stoeckel, Chem. Phys. Lett. 264 (1997) 316–322.

[30] D. Romanini, A.A. Kachanov, F. Stoeckel, Chem. Phys. Lett. 270 (1997) 538–545.

[31] L.S. Rothman, R.L. Hawkins, R.B. Watson, R.R. Gamache, J. Quant. Spectrosc. Radiat. Transfer 48 (1992) 537–566.

[32] A. Chédin, J. Mol. Spectrosc. 76 (1979) 430–491.

[33] Y. Ding, V.I. Perevalov, S.A. Tashkun, J.-L. Teffo, A.-W. Liu, S.-M. Hu, J. Mol. Spectrosc. 222 (2003) 276–283.

[34] S.A. Tashkun, V.I. Perevalov, J.-L. Teffo, Vl.G. Tyuterev, J. Quant. Spectrosc. Radiat. Transfer 62 (1999) 571–598.

[35] S.A. Tashkun, V.I. Perevalov, J.-L. Teffo, L.S. Rothman, Vl.G. Tyuterev, J. Quant. Spectrosc. Radiat. Transfer 60 (1998) 785–801.

[36] S.A. Tashkun, V.G. Tyuterev, in: A.I. Nadezhdinskii, Y.N. Ponomarev, L.N. Sinitsa (Eds.), Proceedings of the 11th Symposium and School on High-Resolution Molecular Spectroscopy, SPIE 2205, 1993, pp. 188–191.

[37] J. Morville, D. Romanini, A.A. Kachanov, M. Chenevier, Appl. Phys. B 78 (2004) 465–476.